Study of structural and magnetic properties of $Fe_{80}P_9B_{11}$ amorphous alloy by *ab initio* molecular dynamic simulation*

Li Zhu(朱力), Yin-Gang Wang(王寅岗)†, Cheng-Cheng Cao(曹成成), and Yang Meng(孟洋)

College of Materials Science and Technology, Nanjing University of Aeronautics and Astronautics, Nanjing 211106, *China*

(Received 11 January 2017; revised manuscript received 28 February 2017; published online 20 April 2017)

The structural and magnetic properties of $Fe_{80}P_9B_{11}$ amorphous alloy are investigated through ab initio molecular dynamic simulation. The structure evolution of $Fe_{80}P_9B_{11}$ amorphous alloy can be described in the framework of topological fluctuation theory, and the fluctuation of atomic hydrostatic stress gradually decreases upon cooling. The left sub peak of the second peak of Fe–B partial pair distribution functions (PDFs) becomes pronounced below the glass transition temperature, which may be the major reason why B promotes the glass formation ability significantly. The magnetization mainly originates from Fe 3d states, while small contribution results from metalloid elements P and B. This work may be helpful for developing Fe-based metallic glasses with both high saturation flux density and glass formation ability.

Keywords: amorphous alloy, *ab initio* molecular dynamic simulation, local atomic structure, magnetic properties

PACS: 71.15.Pd, 75.50.Kj, 64.70.pe **DOI:** 10.1088/1674-1056/26/6/067101

1. Introduction

Due to their excellent soft magnetic property and low cost, Fe-based metallic glasses have captured much attention experimentally and theoretically.[1–6] Metallic glasses are generally produced by rapid cooling methods, where the viscosity increases exponentially until glass transition occurs.[7] Egami *et al*. put forward the concept of atomic level stress, and described the glass transition in terms of topological instability.[8] However, the structure details of metallic glasses remain ambiguous owing to the lack of three-dimensional (3D) atomic structural model. Molecular dynamic (MD) simulation[9] especially *ab initio* molecular dynamic (AIMD) simulation[10] is regarded as an effective way to investigate the structural evolution during rapid cooling on an extremely short timescale.

During the past decades, a lot of work has been done to improve the saturation flux density and the underlying mechanism has been investigated. Earlier study suggested that moment variation in transition metal–metalloid (T-M) alloy is simply determined by the different local symmetry of the M atom or the electronic valence.[11,12] However, these rough approximations could not explain the strong magnetovolume effect observed in Fe-based alloys. Rahman *et al*.[13] studied the influences of impurities in magnetism and electronic structures of bcc Fe. They found that the average magnetic moment generally follows a Slater–Pauling curve, and attributed the discrepancy to the weak ferromagnetic nature of bcc Fe. Recently, Kiss *et al*.[14] investigated the anomalous magnetic behaviors of Fe–Zr metallic glasses in detail and elaborated this anomaly in terms of critical Fe atomic volume. Based on AIMD simulation of $Fe_{85}Si_2B_8P_4Cu_1$ (NANOMET) amorphous alloy,[15] it is revealed that magnetic moment is both electron charge dependent and atomic volume dependent. Our results found that the magnetic moment of Fe of typical Fe-based amorphous alloy $Fe_{80}P_9B_{11}$ is strongly affected by the charge quantity.

2. Simulation details

The calculation was performed by using the Vienna *ab initio* simulation package (VASP).[16] Projected augmented wave (PAW) parameterized by Perdew, Burke, and Ernzerhof was adopted to describe interactions between particles.[17,18] Only Γ-point was used to sample the Brillouin zone. The simulation was performed in a canonical ensemble (NVT) with a Nosé thermostat[19] for temperature control. The initial structure contained 100 atoms that were totally randomly distributed. The melt was kept at 2000 K for 10 ps in time-steps of 5 fs to reach thermal equilibrium. Afterwards, the system was gradually cooled down to 1600 K, 1200 K, 800 K, 600 K, 400 K in 1000 MD steps. The cooling rates were 8×10^{13} K/s and 4×10^{13} K/s when the temperature ranged from 2000 K to 800 K and 800 K to 400 K, respectively. The external pressure was turned to essential zero by adjusting the volume of the supercell. Finally, an additional 5000 MD steps were performed to collect atomic structure information. For accurate electron density of states (DOS) calculation, a $2\times2\times2$ k-points mesh were adopted.

*Project supported by the National Natural Science Foundation of China (Grant No. 51571115) and a Project Funded by the Priority Academic Program Development of Jiangsu Higher Education Institutions.

†Corresponding author. E-mail: yingang.wang@nuaa.edu.cn

© 2017 Chinese Physical Society and IOP Publishing Ltd

3. Results and discussion

The mean square displacements (MSDs) are calculated at each temperature. Using the Einstein relationship: $D = \lim_{t\to\infty}\langle r^2(t)\rangle/6t$, the values of self-diffusion constant D for Fe, P, and B are obtained and shown in Fig. 1. By comparison, the diffusion rates can be ordered as B > P > Fe in magnitude, which is in accord with the results reported previously.[20] It is concluded that glass transition occurs at about 800 K, since the diffusion rate at 800 K is only 4%–6% of that at 2000 K. Figure 2 shows the total pair distribution functions (PDFs) at various temperatures. The positions of first peak of the total PDF are almost the same for various temperatures, while the intensity of first peak slightly increases. Based on topological fluctuation theory,[21] the increase of the intensity of $g(r)$ peak is due to the reduced topological fluctuation. However, the second peak begins to split at about 800 K and the splitting becomes more obvious with the decrease of temperature, which has been reported previously.[22,23] It seems that the left sub peak becomes more prominent with temperature decreasing from 800 K to 400 K, while the right sub peak varies slightly. The relative position of peak at 400 K is approximately 1:1.70:1.96, which follows the universal scaling behaviors of R_i/R_1 pointed out by Liu *et al.*, where R_i is the i-th peak position of PDF.[24] Previous work[25,26] suggested that the unevenness of the connecting style of atomic clusters results in the splitting of the second peak. Thus the liquid–glass transition may be a process of the increase of local topological order combined with the formation of cluster connection.

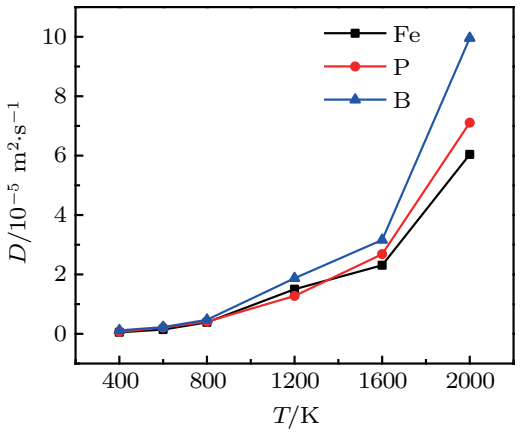


Fig. 1. (color online) Temperature dependence of self-diffusion constant of Fe, P, and B in $Fe_{80}P_9B_{11}$ alloy.

A more detailed study of structure evolution of Fe–P–B amorphous alloy can be done through partial PDFs and the results are shown in Fig. 3. Considering the fact that Fe is the dominating component, only the Fe–Fe, Fe–P, and Fe–B pairs are presented. It can be seen that the Fe–Fe partial PDFs show the same tendency as total PDFs upon cooling. The position of the first peak for Fe–P partial PDF at 400 K is 2.32 Å, which is shorter than the sum of Goldschmidt atomic radii of Fe and P. The first peak of Fe–B partial PDF is located at 2.12 Å, comparable to the sum of Goldschmidt atomic radii of Fe and B. This actually indicates the existence of Fe–P and Fe–B bonds, and the Fe–P bond is stronger than Fe–B bond.[27] It is worth noting that Fe–P pair and Fe–B pair show different behaviors below the glass transition temperature. The left sub peak of the second peak of Fe–B partial PDFs becomes more pronounced, and its position shifts to small value. When a B atom is embedded in Fe-based amorphous matrix, the B atom will suffer compressive stress due to the local topological instability.[8] In addition, the external stress which is equal to the average atomic level stress is zero. Thus, tensile stress is predominant in the second nearest atomic shell and another B atom tends to occupy this site, which may reduce the atomic level stress and hence a denser structure is formed. Dai *et al.*[28] have observed that a positive sign and a negative sign for volumetric strain ε alternate from short range order to medium range order; this phenomenon verifies our findings. In this case, the behavior of Fe–B atomic pair can be attributed to the oscillation of stress (strain). Lashgari *et al.*[29] have reviewed that B can promote the glassy structure to a very great degree. That B can promote the glass formation ability (GFA) of Fe-based amorphous alloy may lie in the unique behavior of Fe–B atomic pair apart from what is so-called "solute–solute avoidance".[27] Because of the relatively large atomic radius of P, this effect is much slighter than that of B.

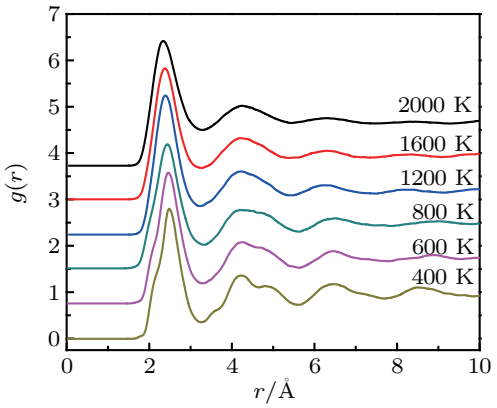


Fig. 2. (color online) Plots of total PDF ($g(r)$) versus position (r) at various temperatures.

The total magnetic moment of our simulated supercell is 165 μ_B. Since it is impossible to contain a domain wall as illustrated by Wang *et al.*,[30] the saturation flux density can thus be calculated from $B_s = M/V = 1.67$ T where B_s, M, and V denote saturation magnetization, calculated magnetic moment, and supercell volume, respectively. Figures 4(a) and 4(b) illustrate total electron DOS and the partial electron DOS of Fe atom in $Fe_{80}P_9B_{11}$ amorphous alloy, respectively. It is obvious that the electron DOS near the Fermi level is dominated by Fe-d states and that the d band splits into two main peaks.

The Fermi level is located right above the majority spin band and falls near the minimum of spin-down band, indicating the existence of ferromagnetism in this alloy. Moreover, both spin bands are partially filled and in this case, exchange splitting energy is less than the energy difference between the Fermi level E_F and the top of the d band. Therefore, $Fe_{80}P_9B_{11}$ alloy is a weak ferromagnet. Figure 5 shows partial DOSs of Fe, P, and B atoms. The s-states of P and B lie far below Fermi level and are fully filled. Besides, there is hybridization between Fe 3d states and 2p states of P and B, which is consistent with the results from partial PDFs. This can explain the small negative magnetic moments of metalloid atoms.

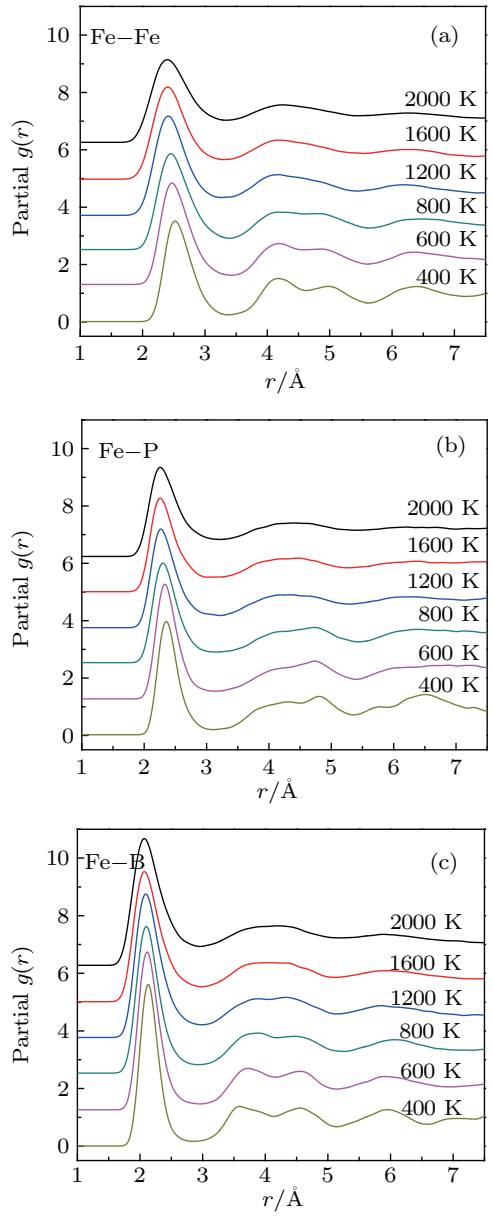


Fig. 3. (color online) Variations of partial PDF $g(r)$ with position for (a) Fe–Fe, (b) Fe–P, and (c) Fe–B atomic pairs at various temperatures.

The average magnetic moments per atom for Fe, P, and B are listed in Table 1. The Fe has an average magnetic moment of 2.1 μ_B, while P and B each obtain a magnetic moment of about -0.1 μ_B. As is well known, the magnetic moment depends on the interplay between a local packing or topologically dependent electronic band structure and the number of valence electrons.[31] The existence of covalent coupling and the larger electronegativity of metalloid atoms result in the charge transfer from Fe atoms to metalloid atoms. The relationship between Fe magnetic moment and charge is illustrated in Fig. 6. One can see that magnetic moment follows nearly linear dependence on charge. The larger the magnetic moment, the less the electric charge quantity that Fe will obtain. Atom-averaged moment in Bohr magnetons is the difference between the atom-averaged number of spin-up and that of spin-down electrons, that is, $\mu_{av} = N^{\uparrow} - N^{\downarrow}$.[9] For systems with strong ferromagnetism whose spin-up d-band is full, and if the contribution from sp-bands is ignored, $N^{\uparrow}$ will be equal to a constant of 5. In this case, the increase of charge indicates the augment of $N^{\downarrow}$, namely the reduction of magnetic moment of Fe. The deviation from linear correlation is due to the fact that $Fe_{80}P_9B_{11}$ amorphous alloy is just a weak ferromagnet so that the magnetic moment is sensitive to the Fe–Fe atomic distance. This can also explain that $Co_{91}Zr_9$ manifests an almost pressure-independent magnetic behavior, while the magnetic property of $Fe_{91}Zr_9$ shows an extreme sensitivity to volume change[14] in this simple method. According to the relevant work,[15] Fe atom pairs with longer distance are supposed to have stronger ferromagnetic exchange, resulting in higher magnetic moment.

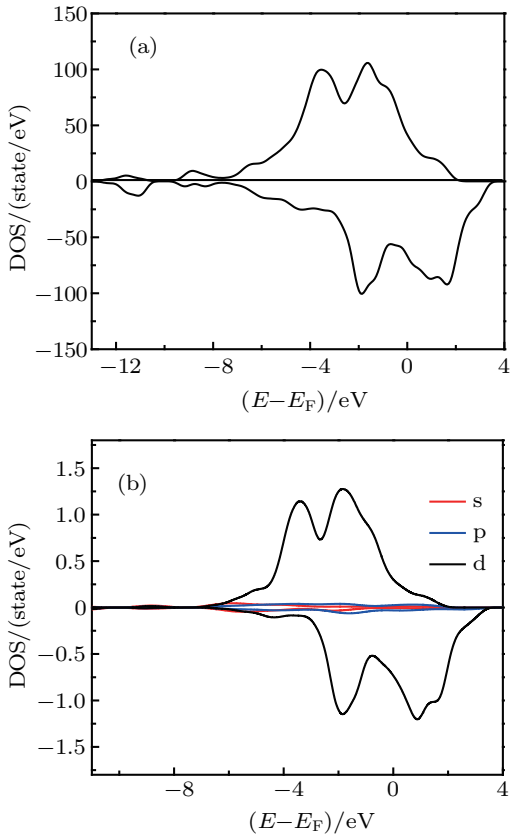


Fig. 4. (color online) (a) Spin-polarized total electron DOS of $Fe_{80}P_9B_{11}$ amorphous alloy, and (b) partial electron DOS of Fe atom.

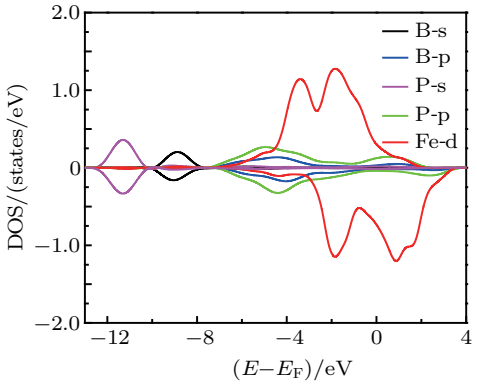


Fig. 5. (color online) Partial DOSs of Fe, P, and B atoms in $Fe_{80}P_9B_{11}$ amorphous alloy.

Table 1. Average magnetic moments m_i $i =$ s, p, and d of s, p, and d states and the total magnetic moments m_{total} of Fe, P, and B atoms in $Fe_{80}P_9B_{11}$ amorphous alloy.

Atom	m_s/μ_B	m_p/μ_B	m_d/μ_B	M_{total}/μ_B
Fe	-0.001	–0.024	2.125	2.100
P	0	–0.105	0.001	–0.104
B	–0.020	–0.104	0.002	–0.121

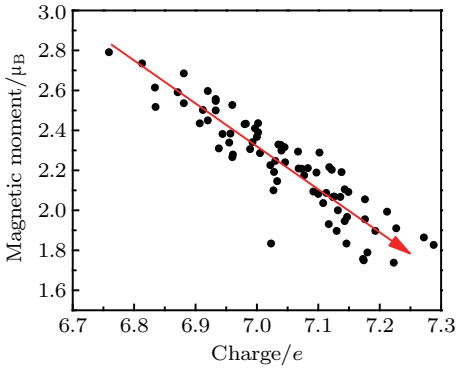


Fig. 6. (color online) Fe magnetic moment versus charge quantity.

The high saturation flux density is preferred for Fe-based metallic glasses. The concentration of Fe atoms dominates the saturation flux density, however, the high concentration of Fe atoms leads to the poor GFA. Therefore, it is worthwhile to investigate the micro-alloying effects in Fe-based amorphous alloys. As discussed above, an alloying element with larger electronegativity may benefit the magnetic property since it will make Fe atoms more positively charged. In contrast, the hybrid Fe–B or Fe–P bonds will replace the polarizable d–d bonds and deteriorate the magnetic property. Therefore there is an optimal concentration of metalloid atoms in Fe-based amorphous alloy to obtain high saturation flux density. To further testify this point, more work needs to be done, and this work provides a theoretic viewpoint for developing Fe-based amorphous alloy.

4. Conclusions

We perform AIMD simulation to investigate the structure evolution of $Fe_{80}P_9B_{11}$ amorphous alloy during rapid cooling and evaluate its magnetic property. It is found the intensity of first $g(r)$ peak increases monotonically with the decrease of temperature. The second peak of PDF starts to split around 800 K. The left sub peak of the second PDF peak of Fe–B becomes more pronounced, and the position shifts to small value below the glass transition temperature, which may be the major reason why B promotes the glass formation ability significantly.

The DOS calculation indicates that the $Fe_{80}P_9B_{11}$ is weak ferromagnet. The calculated average magnetic moment of Fe is about 2.10 μ_B, while P and B obtain the magnetic moments of -0.10 μ_B and -0.12 μ_B, respectively. Our results reveal that in this system, Fe magnetic moment varies almost linearly with electric charge. Alloying elements with large electronegativity may be an effective method of improving the magnetic properties of Fe-based amorphous alloy.

Acknowledgement

The authors thank Prof. P Z Zhang for the valuable discussion.

References

[1] Babilas R 2015 *Mater. Charact.* **107** 7
[2] Bhattacharya S, Lass E A, Poon S J, Shiflet J and Rawlings M 2012 *J. Appl. Phys.* **111** 063906
[3] Zhou S X, Dong B S, Qin J Y, Li D R, Pan S P, Bian X F and Li Z B 2012 *J. Appl. Phys.* **112** 023514
[4] Wang H, Hu T and Zhang T 2013 *Physica B* **411** 161
[5] Gu Y, Chao Y S and Zhang Y H 2012 *Chin. Phys. B* **21** 127805
[6] Han M G, Guo W, Wu Y H, Liu M and Magundappa L H 2014 *Chin. Phys. B* **23** 083301
[7] Cheng Y Q and Ma E 2011 *Prog. Mater. Sci.* **56** 379
[8] Egami T 2011 *Prog. Mater. Sci.* **56** 637
[9] Li J W, Xiao S Y, Xie X X, Yu H, Zhang H L, Zhan Y and An H L 2015 *Chin. Phys. Lett.* **32** 028702
[10] Feng Y X, Chen J, Li X Z and Wang E G 2016 *Chin. Phys. B* **25** 013104
[11] Malozemoff A P, Williams A R and Moruzzi V L 1984 *Phys. Rev. B* **29** 1620
[12] Corb B W, O'Handley R C and Grant N J 1982 *J. Appl. Phys.* **53** 7728
[13] Rahman G, Kim I G, Bhadeshia H K D H and Freeman A J 2010 *Phys. Rev. B* **81** 184423
[14] Kiss L F, Kemeny T, Bednarc J, Gamcova J and Liermann H P 2016 *Phys. Rev. B* **93** 214424
[15] Wang Y C, Takeuchi A, Makino A, Liang Y Y and Kawazoe Y 2014 *J. Appl. Phys.* **115** 173910
[16] Kresse G and Furthmuller J 1996 *Comput. Mater. Sci.* **6** 15
[17] Blochl P E 1994 *Phys. Rev. B* **50** 17953
[18] Kresse G and Joubert D 1999 *Phys. Rev. B* **59** 1758
[19] Nosé S 1984 *J. Chem. Phys.* **81** 511
[20] Wang Y C, Takeuchi A, Makino A, Liang Y and Kawozoe Y 2015 *J. Appl. Phys.* **117** 17B705
[21] Egami T, Poon S J, Zhang Z and Keppens V 2007 *Phys. Rev. B* **76** 024203
[22] Hui X, Fang H Z, Chen G L, Shang S L, Wang Y, Qin J Y and Liu Z K 2009 *Acta Mater.* **57** 376
[23] Xiong L H, Lou H B, Wang X D, Debela T T, Cao Q P, Zhang D X, Wang S Y, Wang C Z and Jiang J Z 2014 *Acta Mater.* **68** 1
[24] Liu X J, Xu Y, Hui X, Lu Z P, Li F, Chen G L, Lu J and Liu C T 2010 *Phys. Rev. Lett.* **105** 155501
[25] Pan S P, Qin J Y, Wang W M and Gu T K 2011 *Phys. Rev. B* **84** 092201
[26] Ding J, Ma E, Asta M and Ritchie R O 2015 *Sci. Rep.* **5** 17429
[27] Zhang W B, Li Q and Duan H M 2015 *J. Appl. Phys.* **117** 104901
[28] Dai J, Wang Y G, Yang L, Xia G T, Zeng Q S and Lou H B 2017 *Scripta Mater.* **127** 88
[29] Lashgari H R, Chu D, Xie S S, Sun H D, Ferry M and Li S 2014 *J. Non-Cryst. Solids* **391** 61
[30] Wang Y C, Zhang Y, Takeuchi A, Makino A, Liang Y Y and Kawazoe Y 2015 *IEEE Trans. Magn.* **51** 2006504
[31] Bakonyi I 2012 *J. Magn. Magn. Mater.* **324** 3961